Preprint Title	Mesoionic tetrazolium-5-aminides: Synthesis, Molecular and Crystal Structures, UV-Vis Spectra, and DFT Calculations
Authors	Vladislav A. Budevich, Sergei V. Voitekhovich, Alexander V. Zuraev, Vadim E. Matulis, Vitaly E. Matulis, Alexander S. Lyakhov, Ludmila S. Ivashkevich and Oleg A. Ivashkevich
Publication Date	22 Oct 2020
Article Type	Full Research Paper
Supporting Information File 1	Suppl_Mesoionic_manuscript.docx; 536.4 KB
ORCID® iDs	Vladislav A. Budevich - https://orcid.org/0000-0003-0729-8869; Sergei V. Voitekhovich - https://orcid.org/0000-0002-7015-5062; Alexander V. Zuraev - https://orcid.org/0000-0001-6933-0524; Vitaly E. Matulis - https://orcid.org/0000-0001-9714-9087

Mesoionic tetrazolium-5-aminides: Synthesis, Molecular and Crystal Structures, UV-Vis Spectra, and DFT Calculations

Vladislav A. Budevich[1]*, Sergei V. Voitekhovich[1], Alexander V. Zuraev[1,2], Vadim E. Matulis[1], Vitaly E. Matulis[1], Alexander S. Lyakhov[1], Ludmila S. Ivashkevich[1] and Oleg A. Ivashkevich[1]

Address: [1]Laboratory for chemistry of condensed systems, Research Institute for Physical Chemical Problems of Belarusian State University, Leningradskaya 14, 220006 Minsk, Republic of Belarus; [2]Inorganic chemistry department, Faculty of Chemistry, Belarusian State University, Nezalezhnastsi avenue 4, 220050 Minsk, Republic of Belarus

_____

Email: Vladislav Aleksandrovich Budevich* – vl.budevich@gmail.com

* Corresponding author

Abstract

Tetrazolium-5-aminides have been prepared by *tert*-butylation of 5-aminotetrazole and its N-methyl derivatives by *t*-BuOH/$HClO_4$ system followed by treatment of tetrazolium salts by alkali. These mesoionic compounds have been found to show higher reactivity of exocyclic N atom in comparison with 5-aminotetrazoles. They react with 1,2-dibromoethane and 5-(methylsulfonyl)-1-phenyl-1*H*-tetrazole and

substitute bromine and methylsulfonyl groups giving tetrazolium salts or conjugate aminides. Obtained mesoionic tetrazoles have been characterized by elemental analysis, FT-IR, NMR and UV-Vis spectroscopy, TGA/DSC analysis and for 1,3-di-*tert*-butyltetrazolium-5-aminide, it's N,N'-ethylene bridged bis-derivative and (1,3-di-*tert*-butyl-*1H*-tetrazol-3-ium-5-yl)(1-phenyl-1*H*-tetrazol-5-yl)amide by single crystal X-ray analysis. Structural and spectral features of tetrazolium-5-aminides are discussed by using quantum-chemical calculations.

Keywords

Aminotetrazoles; DFT; Mesoionic compounds; UV-Vis spectra; X-ray analysis

Introduction

5-Aminotetrazoles are of the most available and valuable tetrazole derivatives. So, due to thermal stability, and high nitrogen content parent 5-aminotetrazole (**1**) (Figure 1) is of practical interest as gas-generator and blowing agent [1, 2]. Moreover, it is a useful building block in organic synthesis, including various multicomponent reactions opening the way to diverse fused heterocycles [3]. Salts with anionic tetrazole, i.e. aminotetrazolates **2**, and cationic one, i.e. aminotetrazolium salts **3**, are attractive as environmentally friendly pyrotechnics [4], insensitive high-energy materials [5–7] and promising energetic ionic liquids [8–10].
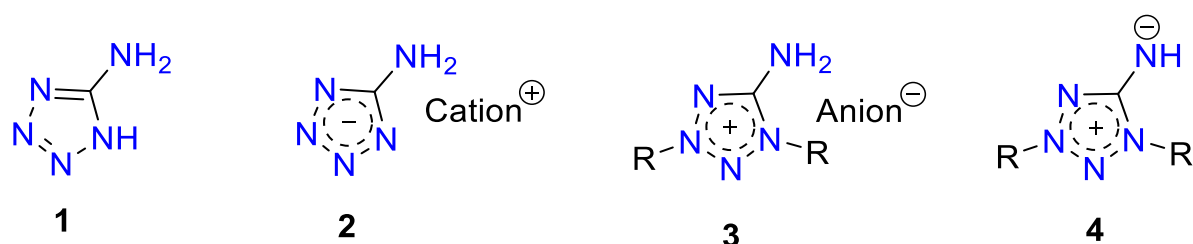

Figure 1: 5-Aminotetrazole derivatives.

The most interesting and less examined 5-aminotetrazole derivatives are tetrazolium-5-aminides, which can be depicted as **4** by analogy with other mesoionic tetrazoles [11, 12]. The first representatives of tetrazole-5-aminides were reported in the 1950s [13, 14], whereas next publications were appeared only five decades later, being devoted to synthesis and photochemistry of 1,3-diaryltetrazolium-5-aminides [15–21]. NMR studies of few tetrazole-5-aminides were carried out as a part of studies of mesoionic compounds [22–24]. Earlier, we reported a facile preparation of 1,3-di-*tert*-butyltetrazolium-5-aminide [25], which was later used for synthesis of the first tetrazolium halocuprate [26]. Very recently, this aminide was found to be suitable ligand for manganese complexes [27] and the agent for preparation of the salt with high energy density [28]. Also, it is worth noting that today only a few examples of mesoionic tetrazole aminides X-ray structures are known [17, 27].
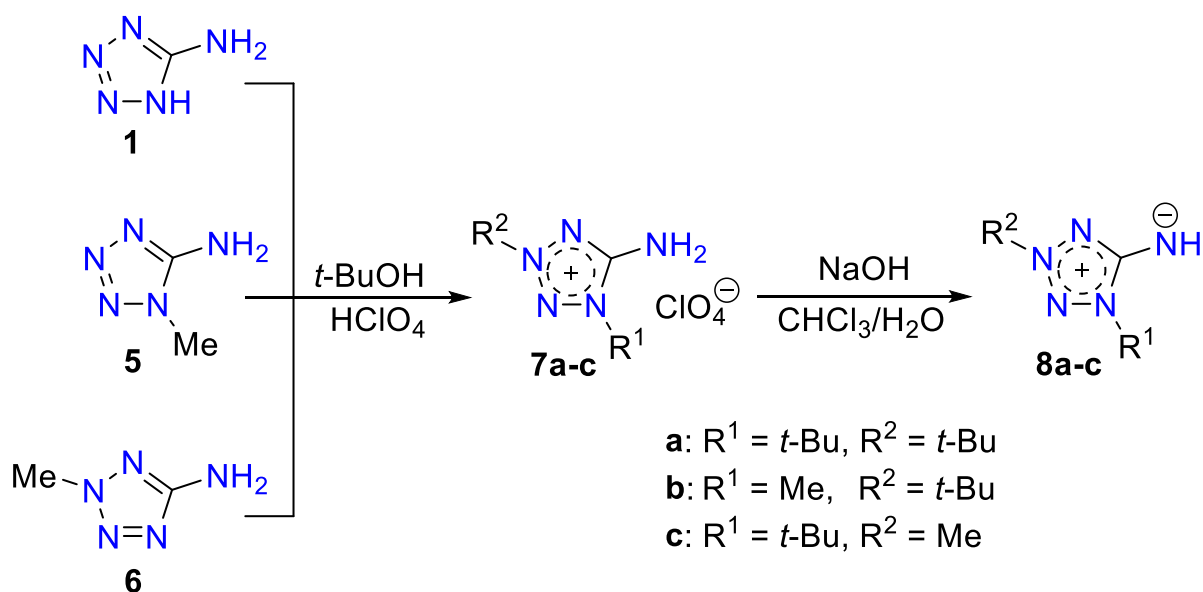
Thus, information on tetrazole-5-aminides is very limited and fragmentary. In the present work, we tried to fill this gap carrying out experimental (synthesis, X-ray, UV-Vis) and theoretical density functional theory (DFT) studies of some 1,3-dialkyltetrazolium-5-aminides.

Results and Discussion

Synthesis and chemical transformations

Tetrazolium-5-aminides can be prepared by three main approaches: a) by deprotonation of 5-aminotetrazolium salts; b) by photochemical transformation of 5-azidotetrazolium salts; c) by functionalization of other aminides. The first way is preferable due to synthetic availability of aminotetrazolium salts [25]. Therefore, here we synthesized 1,3-disubstituted 5-aminotetrazolium perchlorates **7** by quaternization
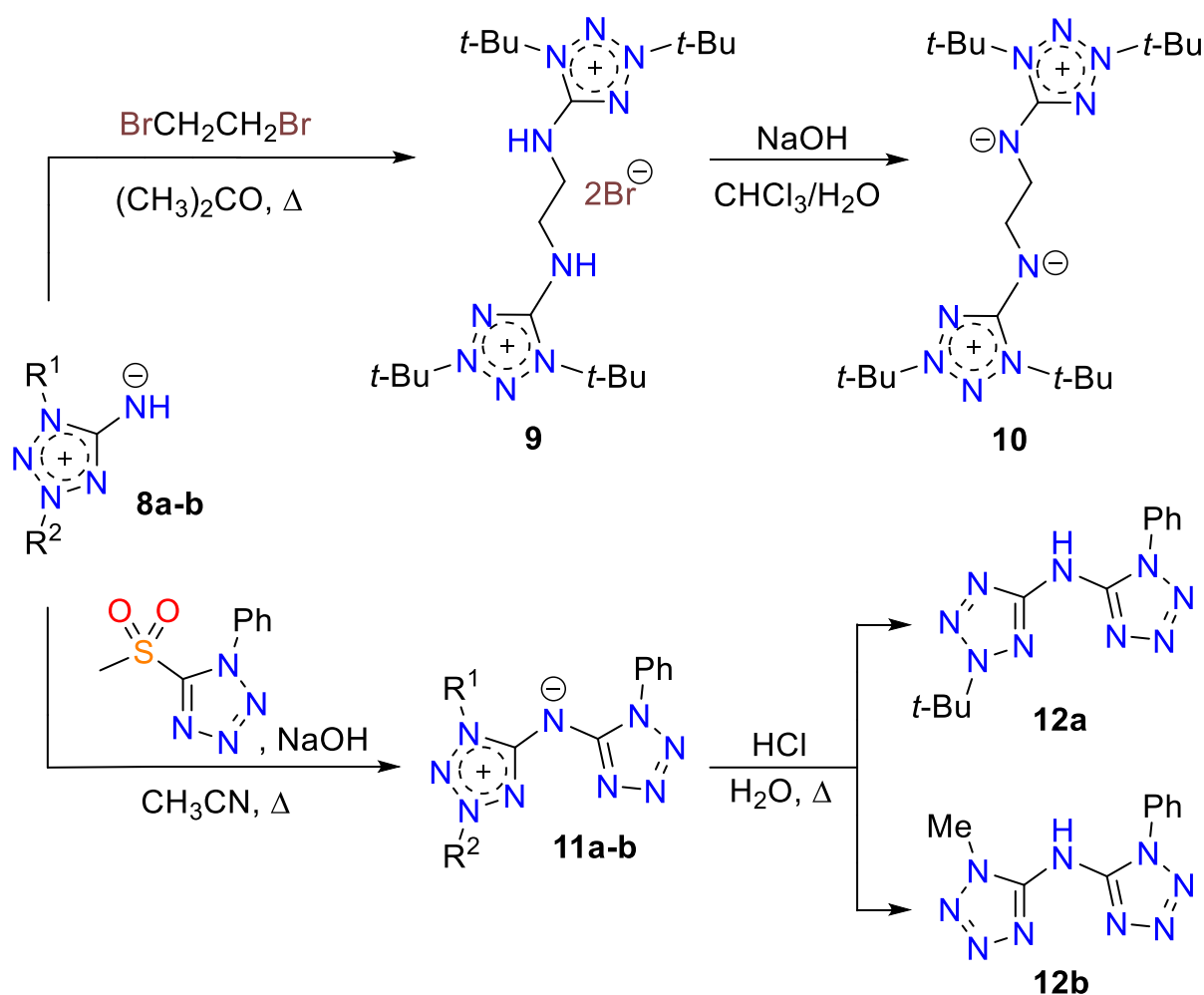
of commercial 5-aminotetrazole (**1**) and its N-methylated derivatives **5** and **6** as shown in Scheme 1. Quaternization proceeded regioselectively using *t*-BuOH/HClO₄ system [25]. Further, salts **7** were treated with sodium hydroxide in the biphasic system water-chloroform giving aminides **8**, which were extracted from reaction mixtures by chloroform.

Scheme 1: Synthesis of tetrazolium-5-aminides.

The obtained aminides **8** are yellow solids soluble in various organic solvents like alcohols, chloroform, dichloromethane, hexane, acetonitrile, toluene, and THF. They are soluble also in water. Remarkably, their solutions in organics are yellow coloured, whereas aqueous solutions are colourless. UV-Vis spectra of **8a** were found to show solvatochromism, discussed in more detail in theoretical section. The ^{13}C NMR shift of C^5 endocyclic atom for aminides **8** is observed at 162.1–163.1 ppm in DMSO-d₆. For parent 5-aminotetrazolium salts, this shift is found at 156.5–158.3 ppm in the same solvent. TGA/DSC data shows thermal stability of tetrazolium-5-aminides (See SI for more details).

Some nucleophlic displacement reactions were carried out in order to show higher reactivity of aminides in comparison to aminotetrazoles. High nucleophility of imine group allows to displace halo- and methylsulfonyl groups by tetrazolium-5-aminide, whereas 5-aminotetrazoles do not react under analogous conditions. So, we prepared bistetrazolium salt **9** by alkylation of aminide **8a** with 1,2-dibromoethane (Scheme 2). The obtained salt **9** was subjected to deprotonation to give bistetrazolium-5-aminide **10**. Reaction of aminide **8a** with 5-methylsulphonyl-1-phenyltetrazole in the presence of sodium hydroxide in boiling acetonitrile was found to yield (1,3-di-*tert*-butyl-1*H*-tetrazol-3-ium-5-yl)(1-phenyl-1*H*-tetrazol-5-yl)amide (**11a**).

Scheme 2: N-Functionalization of 1,3-di-*tert*-butyltetrazolium-5-aminide.

Taking into account the possibility of removing the *tert*-butyl group in tetrazolium salts under acidic conditions [29], N-*tert*-butyltetrazolium-5-aminides are of interest as agents for introduction of tetrazol-5-ylamine groups into various substrates having leaving groups. We carried out de-*tert*-butylation of derivative **11a** under action of hydrochloric acid. De-*tert*-butylation was found to be regioselective leading to 2-*tert*-butyltetrazole derivative **12a** (Scheme 2). Selectivity of this reaction was confirmed by ^{13}C NMR shifts comparison for C^5 endocyclic atoms of tetrazoles **12a** and **12b**: 161.1 and 151.9 ppm for compound **12a**; 153.2 and 151.1 ppm for compound **12b**. It is known that ^{13}C NMR shifts for endocyclic C^5 atom in 2,5-disubstituted tetrazoles is located downfield (162–167 and 151.9 ppm for 2-methyl-5*H*-tetrazole) from the corresponding signal of the 1,5-regioisomers (152–156 and 143.4 ppm for 1-methyl-5*H*-tetrazole) [30]. De-*tert*-butylation selectivity for compound **11b** can be explained by higher stability of *t*-Bu cation versus Me cation.

Crystal structures

Mesoionic compounds **8a**, **10**, **11** and salt **9** were characterized by single crystal X-ray analysis. For all compounds, data collection was performed at a temperature of 100 K. Main crystal data and structure refinement details are given in Table 1.

Mesoionic compounds 8a, 10, and 11. All three compounds are monoclinic, the space groups $P2_1/c$ for **8a** and **10**, and $P2_1/n$ for **11**. The asymmetric units of **8a** and **11** contain one molecule, whereas the unit of **10** includes half molecule. In contrast to **8a** and **11**, the molecule of **10** shows C_i symmetry, with inversion centre lying in the middle of the bond C10–C10^a [symmetry code: (a) $-x+2$, $-y$, $-z+1$]. The structures of the molecules are shown in Figure 2.

Table 1: Single crystal X-ray data and structure refinement details for **8a**, **10, 11**, and **9.**

	8a	10	11	9
Empirical formula	$C_9H_{19}N_5$	$C_{20}H_{40}N_{10}$	$C_{16}H_{23}N_9$	$C_{20}H_{42}Br_2N_{10}$
Formula weight	197.29	420.62	341.43	582.45
Temperature (K)	100(2)	100(2)	100(2)	100(2)
Crystal system	Monoclinic	Monoclinic	Monoclinic	Trigonal
Space group	$P2_1/c$	$P2_1/c$	$P2_1/n$	$R–3$
a (Å)	5.94661(7)	8.23030(10)	9.04560(10)	36.8562(4)
b (Å)	16.2954(2)	10.4082(2)	9.99730(10)	36.8562(4)
c (Å)	12.04281(15)	14.7565(2)	20.0685(3)	12.05390(10)
α (°)	90	90	90	90
β (°)	100.2696(6)	94.5711(7)	100.7743(4)	90
γ (°)	90	90	90	120
V (Å^3)	1148.28(2)	1260.06(3)	1782.83(4)	14180.1(3)
Z	4	2	4	18
d_c (g cm^{-3})	1.141	1.109	1.272	1.228
μ (mm^{-1})	0.074	0.072	0.084	2.596
Crystal size (mm)	0.56×0.31×0.22	0.58×0.50×0.49	0.40×0.28×0.18	0.50×0.10× 0.09
Refl. collected	32431	29074	54434	108400
Refl. independ.	4411	3863	8700	9633

Restraints	0	0	0	0
Parameters	203	196	295	301
GOOF on F^2	1.029	1.072	1.063	1.039
R1/wR2 [I> 2σ(I)]	0.0335/0.0919	0.0371/0.0982	0.0384/0.1027	0.0383/0.0796
R1/wR2 [all data]	0.0361/0.0953	0.0392/0.0998	0.0461/0.1095	0.0639/0.0871
# CCDC	2035296	2035297	2035298	2035299

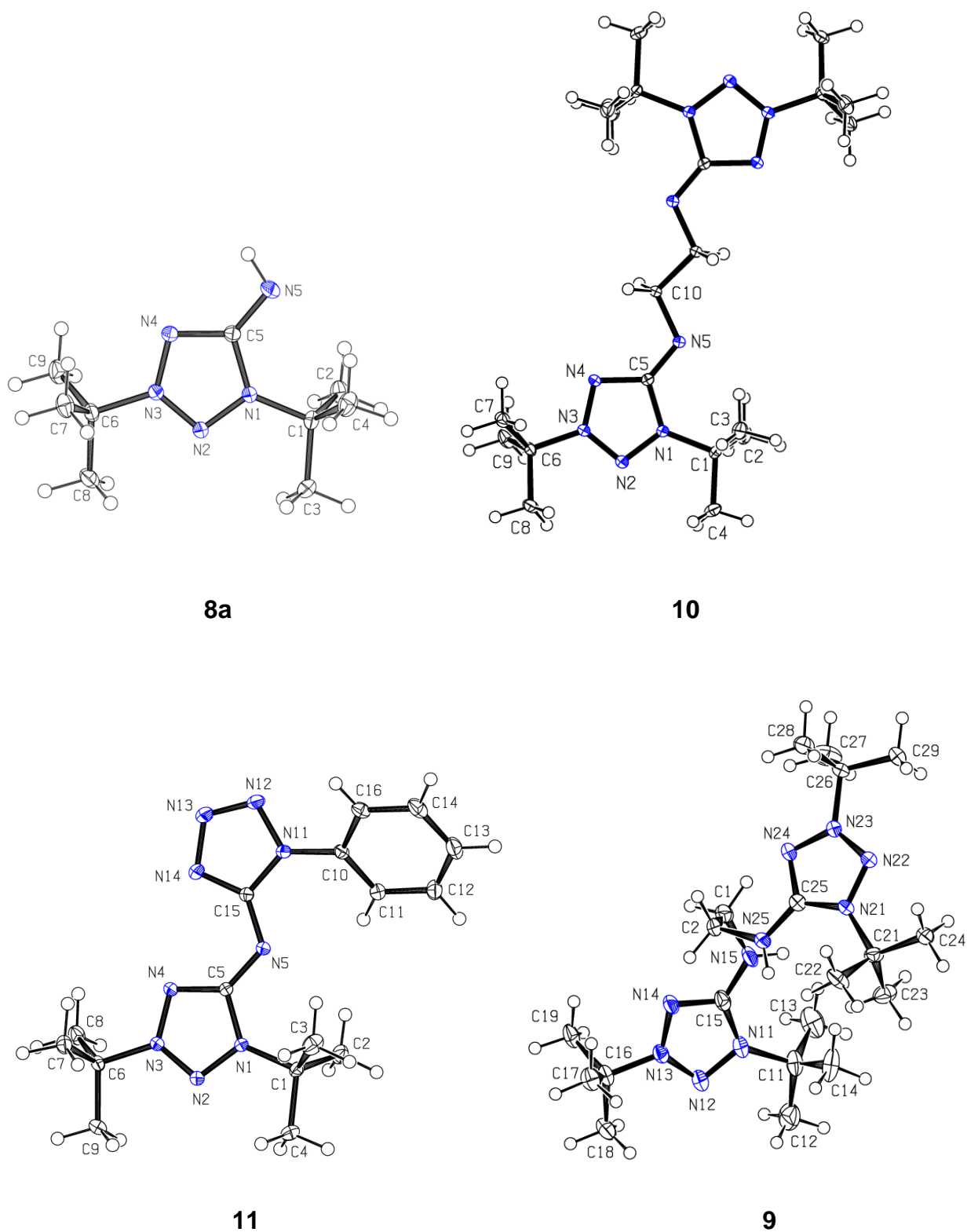**8a**

10

11

9

Figure 2: Molecules of **8a**, **10**, **11**, and bistetrazolium cation in **9**, with displacement ellipsoids drawn at the 50% probability level. The hydrogen atoms are shown as spheres of arbitrary radii. The atom-numbering is done for the asymmetric unit.

Bond lengths in the tetrazole cycles and exocyclic bonds C–N in compounds **8a**, **10**, and **11** are given in Table 2. In these compounds, the shortest bonds are endocyclic N2–N3 and exocyclic C5–N5, being close to double bonds in lengths. However note that the bond C5–N5 in compound **11** is somewhat longer compared to that in **8a** and **10**. This fact can be attributed to some electron density shift in **11** from this bond to the neighboring bond N5–C15, which is exocyclic in the other tetrazole ring N11/C15 and shows the length of 1.3497(7) Å. The longest endocyclic bonds are N1–C5 and N4–C5, lying in the ranges 1.3892(7)–1.4101(9) and 1.3551(7)–1.3784(9) Å, respectively. Remaining bonds N1–N2 and N3–N4 show close lengths, ranged from 1.3333(7) to 1.3419(6) Å.

Table 2: The lengths of the tetrazole ring and exocyclic C–N bonds (Å) in **8a**, **10**, and **11**, and 1,3-di-*tert*-butyltetrazolium-5-aminide ligand in manganese complexes [28].

#	Bond	**8a**	**10**	**11**	Ref. [28]
1	N1–C5	1.4034(6)	1.4101(9)	1.3892(7)	1.386(3), 1.390(3)
2	N1–N2	1.3419(6)	1.3396(8)	1.3333(7)	1.352(3), 1.346(3)
3	N2–N3	1.2937(6)	1.2944(8)	1.2935(7)	1.295(3), 1.291(3)
4	N3–N4	1.3350(6)	1.3397(8)	1.3411(7)	1.331(3), 1.337(3)
5	N4–C5	1.3784(7)	1.3842(9)	1.3551(7)	1.355(3), 1.358(3)
6	C5–N5	1.2986(7)	1.2869(9)	1.3241(7)	1.316(3), 1.315(3)

In Table 2, we presented bond lengths of 1,3-di-*tert*-butyltetrazolium-5-aminide ligand in manganese complex [28], being the only structurally characterized complex with neutral 1,3-di-alkyltetrazolium-5-aminide. Therefore, it is of interest to compare

its structural data with those for **8a** to find the influence of the complexation on the ligand structure. As can be seen, bond lengths of free 1,3-di-*tert*-butyltetrazolium-5-aminide **8a** and the ligand in the manganese complex are rather close. Nevertheless the following structural differences attract the attention. In the complex, endocyclic bonds N1–C5 and N4–C5 are shorter, but exocyclic bond C5–N5 is longer compared to **8a**. One can expect that these structural differences are due to the complexation.

It should be noted that bond lengths of the tetrazole ring N11/C15 in compound **11** are usual for 1- and 1,5-substituted tetrazoles. The compounds **8a**, **10**, and **11** show no hydrogen bonds in their crystal structures, and only van der Waals interactions take place between the molecules.
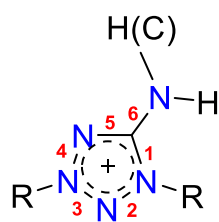
Bistetrazolium salt 9 (bromide salt of mesoionic compound **10**). The compound crystallizes in the trigonal space group *R*–3, with 18 formula units in the unit cell. The asymmetric unit includes one cation, shown in Figure 2, and two bromide anions. The structure of the cation is close to C_2 symmetry, with r.m.s deviation of its non-hydrogen atoms from ideal positions of 0.1320 Å.

In salt **9,** the lengths of the tetrazole ring bonds and exocyclic bond C–N are given in Table 3 together with those in 1,3-di-alkyltetrazolium-5-aminide salts, described in the literature [25–27, 31–34]. First of all, it should be mentioned that the formation of the salt from corresponding mesoionic compound followed by protonation of endocyclic N atom in all cases presented in Table 3. As can be seen, a good agreement of the lengths is observed for each of the six bonds presented in Table 3, and methyl- and *tert*-butyl derivatives show no differences. On the other hand, comparison of the data in Tables 2 and 3 reveals the following structural differences of salts and mesoionic compounds: a) the bonds 1 and 5 in salts are shorter in comparison with mesoionic compounds; b) the bonds 6 (exocyclic C–N)

are somewhat longer in salts. Hence, when the salt is formed the same trends in structural changes in mesoions are observed as under their complexation.

Table 3: The lengths of the tetrazole ring and exocyclic C–N bonds (Å) in salt **9** and corresponding literature data for 1,3-di-alkyltetrazolium-5-aminide salts[a,b].

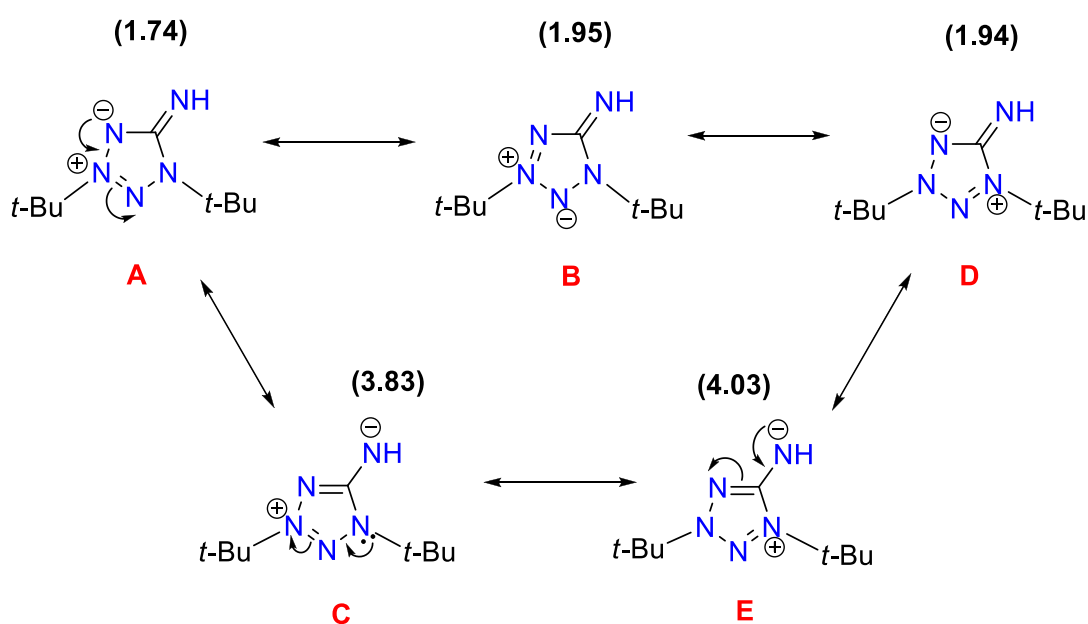| Bond numbering	Bond #	Salt **9**	R = Me Ref. [31–34]	R = t-Bu Ref. [25–27]
	1	1.366(3), 1.359(3)	1.354–1.360	1.365–1.370
	2	1.344(2), 1.347(2)	1.332–1.340	1.340–1.342
	3	1.280(2), 1.286(2)	1.287–1.295	1.284–1.286
	4	1.341(2), 1.336(2)	1.337–1.346	1.334–1.347
	5	1.332(3), 1.333(3)	1.333–1.344	1.332–1.338
	6	1.342(3), 1.334(2)	1.322–1.335	1.322–1.335

[a]Literature data for corresponding bond are given as a range including bond lengths in different salts. [b] Bonds sequence 1–6 correspond to that in Table 2.

In salt **9**, bromide ions are held in the crystal structure by hydrogen bonds N15–H15···Br1[b] [D···A = 3.2774(17) Å, D–H···A = 142°; symmetry code: (b) $-x+y+{}^1/_3$, $-x+{}^2/_3$, $z+{}^2/_3$] and N25–H25···Br2 (D···A = 3.2654(17) Å, D–H···A= 144°). There are also intramolecular hydrogen bonds of the methylene H atoms C2–H2A···N14 [D···A = 3.121(3) Å, D–H···A= 116°].

Theoretical study of structure, UV-Vis spectra and experimental UV-Vis spectra of compound 8a

Quantum-chemical study of structure and UV-Vis spectra, as well as experimental study of UV-Vis spectra were carried out for compound **8a** being the most simple mesoionic compound among investigated in the present work. The atom numbering, used in this Section, corresponds to that in Figure 2. The molecule of **8a** can be represented by several Lewis structures (Scheme 3).

Scheme 3: Possible Lewis structures for the molecule of **8a**, with non-Lewis occupancies as % of total electron density (given in parentheses).

To find the best Lewis structure for the molecule of **8a**, the natural bond orbital (NBO) analysis was applied. In terms of NBO theory, the "best Lewis structure" is the structure with the lowest non-Lewis occupancy. The NBO search for the molecule of **8a** led to the best Lewis structure **A** (Scheme 3). High non-Lewis occupancy shows a strong electron delocalization in the molecule of **8a**. To study the nature of the electron delocalization for the structure **A,** an analysis of the interactions between

donor Lewis-type NBOs and acceptor non-Lewis NBOs was performed. It showed that p-type lone pair on N4 atom is strongly delocalized into vicinal N2−N3* and C5−N5* antibonds, leading to Lewis structures **B** and **C**, correspondingly (Scheme 3). A similar analysis of donor-acceptor interactions for the obtained structures leads to Lewis structures **D** and **E**. Note that the structures **B** and **D** with double C5−N5 bonds have only slightly higher non-Lewis occupancy in comparison with **A**, and hence they are also good Lewis structures. Thus, the structures **A**, **B**, and **D** make a greater contribution to the overall structure of **8a** in comparison with structures **C** and **E** with single C5−N5 bonds.
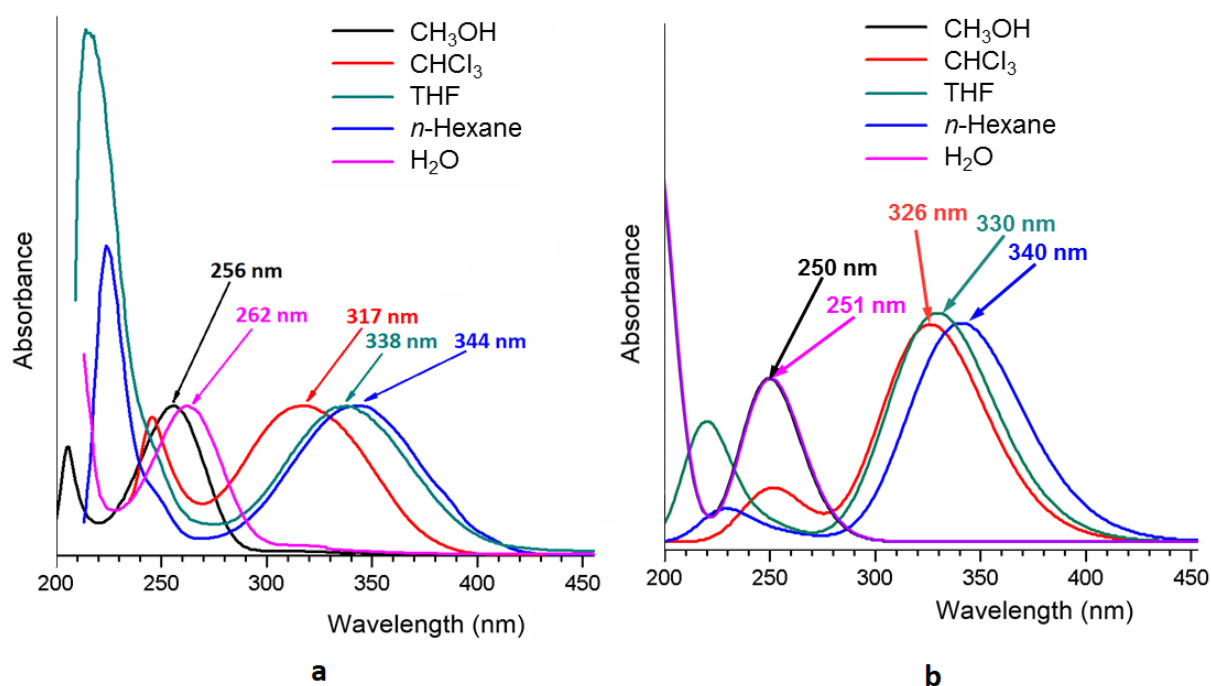

Figure 3: Experimental (a) and TD-tHCTHhyb/6-311+G(2d,p) calculated (b) UV-Vis spectra of **8a** in different solvents. Model structures of **8a**, shown in Figure 4, are used in the calculations.

As mentioned above, compounds **8a-c** show solvatochromism. The experimental UV-Vis spectra of **8a** in different solvents are presented in Figure 3a. As can be seen, the experimental spectra in *n*-hexane and THF, being similar, differ significantly from those in chloroform, methanol, and water. This difference may be due to the following reasons: in the case of chloroform, solvent can form hydrogen bonds with nitrogen atoms of the **8a** molecule; for methanol and water solutions, solvent can be a donor of proton, as a result, **8a** may exist in 1,3-di-*tert*-butyl-5-aminotetrazolium cation form. To confirm this assumption, we calculated UV-Vis spectra of **8a** in different solvents for model structures shown in Figure 4. The model structures in Figure 4b and 4c were built based on the results of our calculations of NPA charges and molecular electrostatic potential (MESP) (Figure 5), showing that the largest negative charge and the deepest minimum of MESP of **8a** are located near the exocyclic atom N5, and hence it is the most preferable protonation site in **8a**.
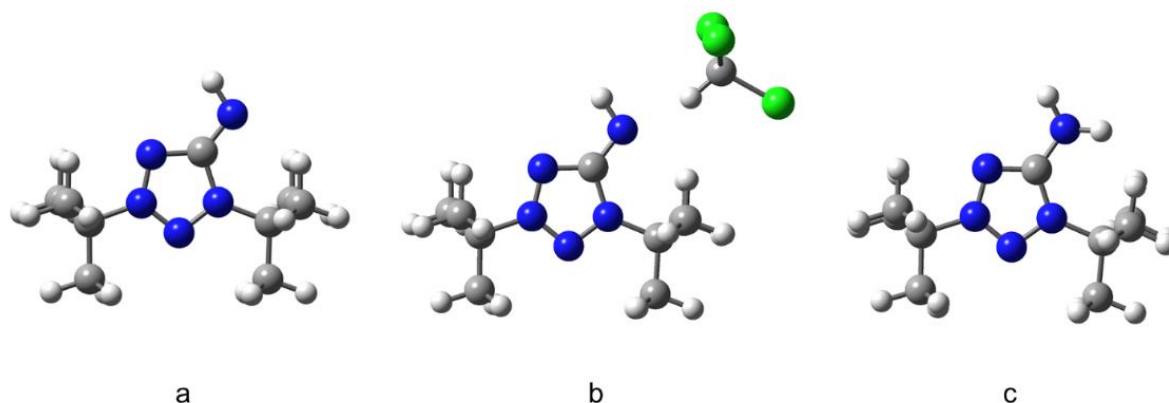

a   b   c

Figure 4: Model structures of **8a** used for calculations of the UV-Vis spectra: a) in *n*-hexane and THF; b) in chloroform; c) in methanol and water.
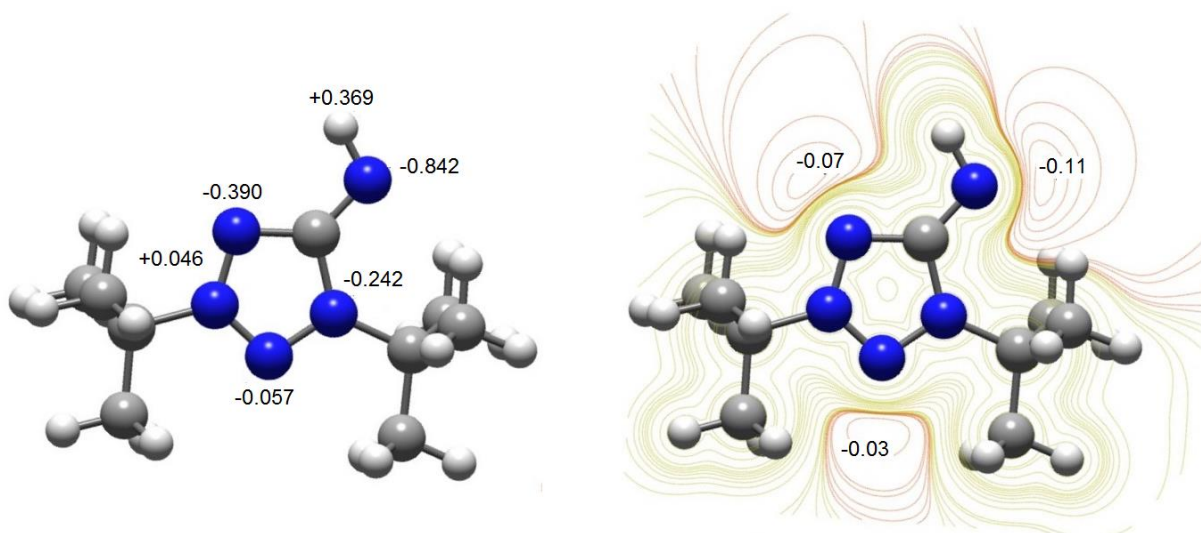
Figure 5: NPA charges (left) and MESP contour map (right) for the molecule of **8a**.

TD-tHCTHhyb/6-311+G(2d,p) calculated UV-Vis spectra of **8a** in *n*-hexane, THF, chloroform, methanol and water are presented in Figure 3b. As can be seen, for *n*-hexane and THF solutions, the experimental and calculated spectra are in a good agreement in the case of model structure in Figure 4a. In the case of chloroform solution, the calculated spectrum agrees with the experimental one only if the formation of a hydrogen bond between exocyclic N5 atom and the solvent is taken into account (model structure in Figure 4b). For methanol and water solutions, the agreement between the calculated and experimental spectra is observed only when the protonation of N5 atom is taken into account (model structure in Figure 4c). For more details, see supplementary materials.

Charge transfer (CT) during the excitation plays a key role in many technological applications because CT states correspond to a light activated electron-hole separation where the positive and negative charges are distant enough to allow their independent collection. In this case, the charge goes from a Donor–Acceptor (S0) to a Donor(+)-Acceptor(–) (S1). We have studied how the nature of solvent can

influence S0→S1 CT. For this purpose, we calculated plots of highest occupied molecular orbital (HOMO), lowest unoccupied molecular orbital (LUMO), electron density difference between S1 and S0 states, as well as S0→S1 CT for **8a** in non-polar *n*-hexane (Figure 6) and polar water solution (Figure 7).

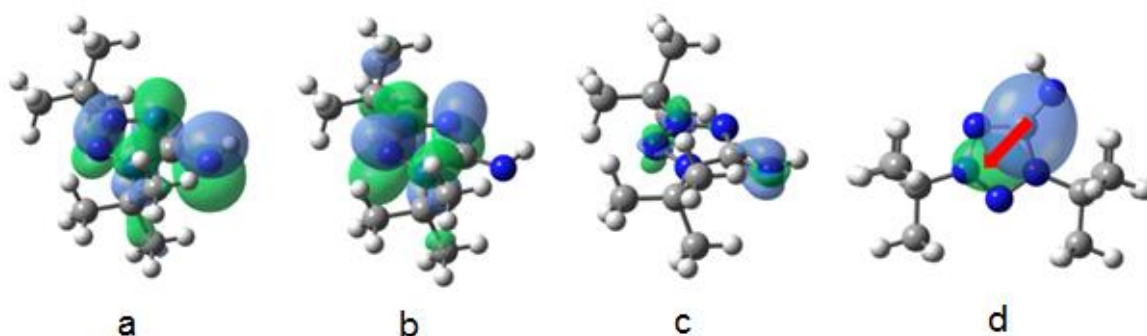**Figure 6**: The calculated in *n*-hexane plots of: a) HOMO; b) LUMO; c) electron density difference between S1 and S0 states; d) S0→S1 CT. Green (blue) regions (for c and d) indicate an increase (decrease) in the electron density upon electronic transition. The red arrow shows the charge transfer.

Figure 7: The calculated in water plots of: a) HOMO; b) LUMO; c) electron density difference between S1 and S0 states; d) S0→S1 CT. Green (blue) regions (for c and d) indicate an increase (decrease) in the electron density upon electronic transition. The red arrow shows the charge transfer.
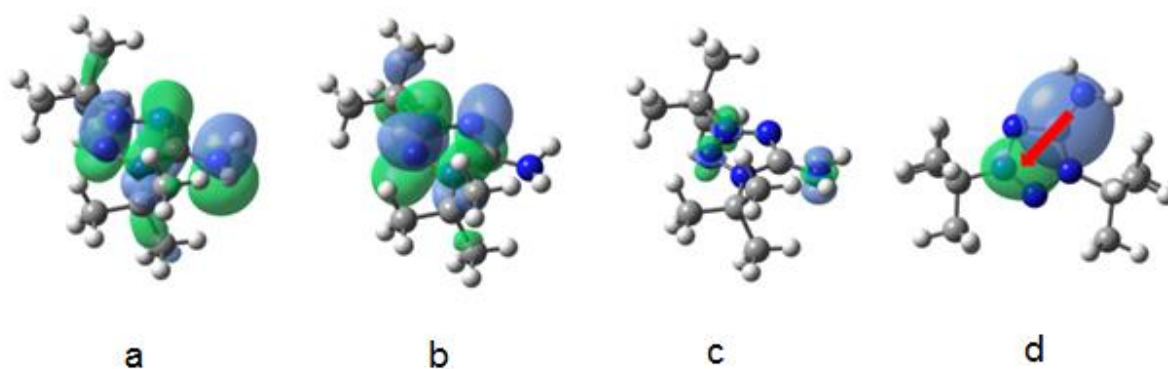
As it can be seen from HOMO, LUMO and electron density difference plots, S0→S1 electron excitation corresponds to π→π* transition in *n*-hexane solution (Figure 6a-c) and to n→π* transition in water solution (Figure 7a-c). In both cases, the transition accompanied by CT from =N5–H group (Donor) to the tetrazole ring (Acceptor) (Figures 6d and 7d). For *n*-hexane and water solutions, the calculated CT distances are 1.5 and 2.0 Å, respectively. The change in the dipole moment, caused by the excitation, is greater in water being of 6.1 D *vs* 4.9 D in *n*-hexane. Moreover, the calculated *т* index is much greater in the case of water solution (0.520 Å in water *vs* 0.017 Å in *n*-hexane). Note, that greater positive *т* index indicates stronger charge separation as a result of the electron transition [35]. Hence, in the case of *n*-hexane, distribution of positive and negative charge is almost not separated, and CT is small. But, for water solution, distribution of positive and negative charge is significantly separated due to strong CT.

Considering that in polar media S0→S1 electron excitation corresponds to n→π* transition, leading to significant CT from =N5–H group to the tetrazole ring, we can explain the strong blue shift, observed in methanol and water solution. So, in the ground state, the N5 atom of **8a** has large negative charge (Figure 5) and strongly interacts with polar solvents. Therefore, polar solvents significantly decrease the ground state energy. When the excited state emerges, the strong CT from =N5–H group to the tetrazole ring (Figure 6c and d) leads to decrease in electronic density on N5 atom. The solvent molecules do not have time to rearrange in order to stabilize the excited state. This results in lower ground state energy, but not the excited state. Therefore, the energy of S0→S1 transition increases, and blue shift is observed in polar media.

Conclusion

Mesoionic tetrazolium-5-aminides can be easily prepared by alkylation of available 5-aminotetrazole and its N-alkyl derivatives in t-BuOH/HClO$_4$ system followed by treatment of tetrazolium salts by alkali. These mesoionic compounds show higher reactivity of exocyclic N atom in comparison with 5-aminotetrazoles ones that can be explained by unique mesoionic system of tetrazolium-5-aminides which lead up to 5-aminogroup activation. They react with 1,2-dibromoethane and 5-(methylsulfonyl)-1-phenyl-1H-tetrazole and substitute bromine and methylsulfonyl groups giving tetrazolium salts or conjugate aminides. Obtained mesoionic tetrazoles have been characterized by elemental analysis, FT-IR, NMR and UV-Vis spectroscopy, TGA/DSC analysis and for 1,3-di-*tert*-butyltetrazolium-5-aminide, it's N,N'-ethylene bridged bis-derivative and (1,3-di-*tert*-butyl-*1H*-tetrazol-3-ium-5-yl)(1-phenyl-1*H*-tetrazol-5-yl)amide by single crystal X-ray analysis. Structural and spectral features of tetrazolium-5-aminides are discussed by using quantum-chemical calculations.

Experimental

CAUTION: The prepared 5-iminotetrazoles and its derivatives are energetic compounds with increased sensitivities against heat. Although we had no problems in synthesis, the use of safety equipment such as leather gloves, face shield and use of Teflon spatulas is mandatory.

General information

Unless otherwise noted, all reagents were obtained from commercial sources and used without further purification. UV-Vis spectra were recorded on Merertech SP-8001-6C UV/Visible spectrophotometer. ^{1}H and ^{13}C NMR spectra were recorded on a

Bruker AVANCE 500 MHz spectrometer. IR spectra were recorded on Bruker Vertex 70 spectrometer in diamond cell accessory. For Raman spectra registration, Ocean Optics ID RAMAN READER (785 nm) spectrometer was used.

Experimental procedures

Experimental procedures are given in supplementary.

Computation details

Calculations of the UV-Vis spectra and charge transfer were carried out within density functional theory for ground states and time-dependent density functional theory (TD-DFT) for excited states using τ-dependent hybrid tHCTHhyb functional [36] with 6-311+G(2d,p) basis set [37]. Chosen functional allows predict valence electronic transition energies with high accuracy [38]. However, tHCTHhyb functional is much less accurate in calculation of Rydberg electronic transition energies [38]. Geometry of **8a** was fully optimized for the ground state in each solvent – n-hexane, THF, chloroform, methanol, water. Solvation effects were considered using SMD [39] model in terms of Linear Response scheme [40]. The analysis of charge transfer during S0→S1 transition was carried out using Multiwfn software [35].

The NBO analysis and MESP calculations were performed using B3LYP/6-31G(d) level of theory [41].

X-ray Structure Determination

Single crystal X-ray diffraction data of mesoionic compounds **8a**, **10**, **11** and salt **9** were collected on a SMART Apex II diffractometer using graphite monochromated Mo-Kα radiation (λ = 0.71073 Å) at a temperature of 100 K. The structures were solved by direct methods (SIR2014) [42] and refined on F^2 by the full-matrix least

squares technique (SHELXL 2014) [43]. The intensities were corrected for absorption. For all compounds, non-hydrogen atoms were refined anisotropically. For compounds **8a**, **10**, and **11**, all hydrogen atoms were found from difference Fourier map. For **8a**, they were refined isotropically; for **10** and **11**, positions of hydrogen atoms were refined with $U_{iso}(H) = 1.5U_{eq}(C)$ for the methyl groups and $U_{iso}(H) = 1.2U_{eq}(C)$ for others. For salt **9**, the methyl and methylene groups H atoms were placed in calculated position and refined in a "riding model", with $U_{iso}(H) = 1.5U_{eq}(C)$ for the methyl and $U_{iso}(H) = 1.2U_{eq}(C)$ for the methylene groups; the hydrogen atoms of N–H groups were found from difference Fourier map and refined isotropically with $U_{iso}(H) = 1.2U_{eq}(N)$. In salt **9**, the structure contains large voids, however the residual electron density in the voids was difficult to model and therefore, the SQUEEZE routine in PLATON [44] was used to remove the contribution of the electron density in the solvent region from the intensity data and the solvent-free model was employed for the final refinement. The solvent contribution was not included in the reported molecular weight and density. Molecular graphics was performed with the programs ORTEP-3 for Windows [45] and PLATON [46]. CCDC deposition numbers for the compounds: 2035296 (**8a**), 2035297 (**10**), 2035298 (**11**), 2035299 (**9**).

Supporting Information

Supporting information text

Supporting Information File 1:

File Name: Suppl_Mesoionic_manuscript

File Format: .docx

Title: Supplementary materials

ORCID IDs

Vladislav A. Budevich – http://orcid.org/0000-0003-0729-8869

Sergei V. Voitekhovich – https://orcid.org/0000-0002-7015-5062

Alexander V. Zuraev – http://orcid.org/0000-0001-6933-0524

Vadim E. Matulis – https://orcid.org/0000-0002-9163-7810

Vitaly E. Matulis – https://orcid.org/0000-0001-9714-9087

Alexander S. Lyakhov – https://orcid.org/0000-0003-4782-4974

Ludmila S. Ivashkevich – http://orcid.org/0000-0001-5114-8628

and Oleg A. Ivashkevich – https://orcid.org/0000-0002-5006-2715

References

1. Lesnikovich, A. I.; Ivashkevich, O. A.; Levchik, S. V.; Balabanovich, A. I.; Gaponik, P. N.; Kulak, A. A. *Thermochim. Acta* **2002**, *388*, 233–251.

2. Han, Z. Y.; Zhang, Y. P.; Du, Z. M.; Li, Z.Y.; Yao Q.; Yang Y. Z. *J. Energ. Mater*., **2018**, *36,* 61–68.

3. Dolzhenko, A. V. *Heterocycles*, **2017**, *94*, 1819–1846.

4. Ernst, V.; Klapötke, T. M.; Stierstorfer J. *Z. Anorg. Allg. Chem.,* **2007**, *633*, 879–887.

5. Karaghiosoff, K.; Klapötke, T. M.; Mayer, P.; Sabate, C. M.; Penger, A.; Welch, J. M. *Inorg. Chem.,* **2008**, *47*, 1007–1019.

6. Kumbhakarna N.; Thynell, S.T. *Thermochim. Acta*, **2014**, *582*, 25–34.

7. Brill T.; Ramanathan H. Combust. Flame, **2000**, *122,* 165–171.

8. Singh, R. P.; Verma, R. D.; Meshri, D. T.; Shreeve, J. M. *Angew. Chem., Int. Ed.,* **2006**, *45*, 3584–3601.

9. Tao, G.-H.; Tang, M.; He, L.; Ji, S.-P.; Nie F.-D.; Huang, M. *Eur. J. Inorg. Chem.*, **2012**, 3070–3078.

10. Tao, G.-H.; Guo, Y.; Joo, Y.-H.; Twamley, B.; Shreeve, J.M. *J. Mater. Chem.*, **2008**, *18*, 5524–5530.

11. Ollis, W. D.; Ramsden, C. A. *Adv. Heterocycl. Chem.*, **1976**, *19*, 1–122.

12. Moderhack, D. *Heterocycles*, **2016**, *92*, 185–233.

13. Bryden, J. H.; Henry, R. A.; Boschan, R.; McEwan, W. S.; Van Dolah, R. W. *Am. Chem. Soc.*, **1953**, *75*, 4863–4864.

14. Henry, R. A.; Finnegan, W. G.; Lieber E. *J. Am. Chem. Soc.*, **1954**, *76*, 2894–2898.

15. Araki, S.; Kuzuya, M.; Hamada, K.; Nogura, M.; Ohata, N. *Org. Biomol. Chem.*, **2003**, *1*, 978-983.

16. Araki, S.; Hattori, H.; Ogawa, K.; Kuzuya, M.; Inoue, T.; Yamamura, H.; Kawai, M. *J. Chem. Soc., Perkin Trans. 1*, **2001**, 2476–2482.

17. Araki, S.; Hattori, H.; Yamamura, H.; Kawai, M. *J. Heterocycl. Chem.,* **2000**, *37*, 1129–1134.

18. Araki, S.; Yamamoto, K.; Inoue, T.; Fujimoto, K.; Yamamura, H.; Kawai, M.; Butsugan, Y.; Zhou, J.; Eichhorn, E.; Rieker, A.; Huber, M. *J. Chem. Soc., Perkin Trans. 2,* **1999**, 985–995.

19. Araki, S.; Hattori, H.; Shimizu, N.; Ogawa, K.; Yamamura, H.; Kawai, M. *J. Heterocycl. Chem.,* **1999**, *36*, 863–867.

20. Araki, S.; K. Yamamoto, M. Yagi, T. Inoue, H. Fukagawa, Hattori, H.; Yamamura, H.; Kawai, M.; Butsugan, Y. *Eur. J. Org. Chem.,* **1998**, 121–127.

21. Bocian, W.; Jaźwiński, J.; Koźmiński, W.; Stefaniak, L.; Webb, G. A. *J. Chem. Soc., Perkin Trans. 2*, **1994**, 1327–1332.

22. Jaźwiński, J.; Rozwadowski, Z.; Magiera, D.; Duddeck, H. *Magn. Reson. Chem.,* **2003**, *41*, 315–323.

23. Jaźwiński, J.; Staszewska, O.; Stefaniak, L.; Araki S.; Webb, G. A. *J. Mol. Struct.,* **2000**, *523*, 103–107.

24. Jaźwiński, J. *Polish J. Chem.,* **1999**, *73*, 1719–1724.

25. Voitekhovich, S. V.; Gaponik, P. N.; Lyakhov, A. S.; Ivashkevich, O. A. *Tetrahedron*, **2008**, *64*, 8721–8725.

26. Voitekhovich, S. V.; Lyakhov, A. S.; Ivashkevich, L. S.; Schleife, F.; Schnorr, R.; Kersting, B.; Gaponik, P. N. *Inorg. Chim. Acta*, **2014**, *419*, 124–129.

27. Vaddypally, S.; Tomlinson, W.; O'Sullivan, O. T.; Ding, R.; Van Vliet, M.; Wayland, B. B.; Hooper, J. P.; Zdilla, M. J. *J. Am. Chem. Soc.*, **2019**, *141,* 5699–5709.

28. O'Sullivan, O. T.; Zdilla, M. J. *Chem. Eur. J.,* **2017**, *23*, 14138–14142.

29. Voitekhovich, S. V.; Gaponik, P. N.; Ivashkevich, O. A. *Russ. Chem. Rev.,* **2002**, *71*, 721–739.

30. Ostrovskii, V. A.; Koldobskii, G. I.; Trifonov, R. E. *In Comprehensive Heterocyclic Chemistry III*; Katritzky, A. R.; Ramsden, C. A.; Scriven, E. F. V.; Taylor, R. J. K.; Zhdankin, V. V. Eds.; Elsevier: Oxford, Tokyo, **2008**; *vol. 6*, 257–423.

31. Klapotke, T. M.; Sabate, C. M.; Rusan, M. *Z. Anorg. Allg. Chem.* **2008**, *634*, 688–695.

32. Klapotke, T. M.; Sabate, C. M. *New J. Chem.*, **2009**, *33*, 1605–1617.

33. Klapotke, T. M.; Sabate, C. M. *Eur. J. Inorg. Chem.*, **2008**, 5350–5366.

34. Klapotke, T. M.; Sabate, C. M.; Penger, A.; Rusan, M.; Welch, J. M. *Eur. J. Inorg. Chem.*, **2009**, 880–896.

35. Tian, L.; Feiwu, Ch. *J. Comput. Chem.,* **2012**, *33,* 580–592.

36. Boese, A. D.; Handy, N. C. *J. Chem. Phys.*, **2002**, *116*, 9559–9569.

37. McLean, A. D.; Chandler, G. S. *J. Chem. Phys.*, **1980**, *72*, 5639–5648.

38. Isegawa, M.; Peverati, R; Truhlar, D. G. *J. Chem. Phys.*, **2012**, *137*, 244104–244117.

39. Marenich, A. V.; Cramer, C. J.; Truhlar, D. G. *J. Phys. Chem.*, **2009**, *113*, 6378–6396.

40. Cammi, R.; Mennucci, B. *J. Chem. Phys.*, **1999***, 110*, 9877–9886.

41. Becke, D. *J. Chem. Phys.*, **1993**, *98*, 5648–5652.

42. Burla, M. C.; Caliandro, R.; Carrozzini, B.; Cascarano, G. L.; Cuocci, C.; Giacovazzo, C.; Mallamo, M.; Mazzone, A.; Polidori, G. *J. Appl. Crystallogr.* **2015.** *48*, 306–309.

43. Sheldrick, G. M. *Acta Crystallogr. Sect. C: Cryst. Struct. Commun.* **2015**, *71*, 3–8.

44. Spek*, A. L. *Acta Crystallogr. Sect. C: Struct. Chem.* **2015**, *71*, 9–18.

45. Farrugia, L. J. *J. Appl. Crystallogr.* **1997**, *30*, 565.

46. Spek*, A. L. *Acta Crystallogr. Sect. D: Biol. Crystallogr.* **2009**, *65*, 148–155.